Potential Energy Surfaces and Dynamical Behavior of Two Rigidly Linked Bichromophoric Molecules Studied by CASSCF Computations and Ab Initio Classical Trajectory Simulations

Franck Jolibois,*,† Michael J. Bearpark,‡ and Michael A. Robb‡

Laboratoire de physique quantique, IRSAMC, 118 route de Narbonne, 31062 Toulouse Cedex, France, and Department of Chemistry, King's College London, Strand, London, WC2R 2LS United Kingdom

Received: October 22, 2001; In Final Form: March 7, 2002

Potential energy surface analysis and classical trajectory simulations have been used to study intramolecular electronic energy transfer (IEET) in two aliphatic diketones that each contains two rigidly linked carbonyl chromophores. This article provides evidence that two geometric coordinates (the carbonyl bond lengths) and two singlet diabatic states (characterized by specific excitation of either one carbonyl chromophore or the other) are needed to understand the mechanism of IEET in these systems. Although computations show that a nonadiabatic transition step is involved in the process, IEET is mainly an adiabatic mechanism of intramolecular vibrational redistribution (IVR) on the lowest excited state into the vibrations of the chromophore that is not initially excited. Dynamics calculations show that this redistribution is slower in the molecule characterized by the more extended σ-bond bridge. It is demonstrated that the σ-bond bridge not only enhances interchromophoric electronic coupling via through-bond interactions compared to through-space interactions, it also controls the IEET process by promoting IVR from one side of the molecule into the other.

Introduction

A bichromophoric molecule (D−B−A) is characterized by two distinguishable chromophores (D and A) connected by a molecular bridge (B). The bridge acts as a molecular spacer and determines the flexibility of the whole bichromophoric system. In such molecules, intramolecular electronic energy transfer (IEET) is a photophysical process that occurs between the two chromophores. The excitation energy is transferred from an excited-state donor D* to a ground-state acceptor A, resulting in quenching of D* fluorescence and sensitization of A. This process is involved in photosynthesis, light harvesting, polymer photophysics and photochemical synthesis and thus is of fundamental importance in biology, chemistry and physics.[1]

The rates of IEET processes are usually interpreted in terms of phenomenological models such as the modified Fermi golden rules proposed by Förster[2−4] and Dexter.[5] A good discussion of these theories can be found in the review of Speiser.[1] In these models, the rate of the IEET process is correlated with vibrational wave function overlaps, long-range Coulombic forces and dipole−dipole interactions. Förster's model generally applies for long-range Coulombic interactions when dipole−dipole transitions are allowed.[2−4] On the other hand, a short-range through-space Dexter-type exchange interaction may be necessary to understand IEET processes involving forbidden transitions.[5] However, in many experimental cases, the observations do not fit with either the Förster or Dexter models and thus another mechanism, the so-called through-bond superexchange interaction, is often invoked.[6−15] This mechanism is experimentally characterized by an interchromophoric distance (R) dependence of the efficiency of the process that does not follow either Förster or Dexter theories. While for flexible molecules IEET remains controlled mostly by a short-range Dexter-type interaction, in rigidly linked structures this process is still efficient at long distance ($R > 10$ Å) for dipole−dipole forbidden processes (see ref 1 and other references therein).

Schippers and Dekkers have reported measurements on two diketones that contain two carbonyl groups in twisted cyclopentane rings of opposite chirality, namely the *trans*-bicyclo-[3.3.0]octane-3,7-dione (BOD) and the (1*S*,3*R*,7*R*,9*S*)-tricyclo-[7.3.0.0]dodecane-5,11-dione (TDD).[16]

While each molecule has a meso structure (*RS*) in its ground state, excitation to the first singlet $n \rightarrow \pi^*$ excited state leads to two enantiomeric forms, *R***S* and *RS**, provided the excitation energy is localized at one or other carbonyl groups. The intramolecular energy transfer process that occurs after $n \rightarrow \pi^*$ excitation has been studied by using circularly polarized light (CPL) (See Scheme 1.) By exciting each molecule at 310 nm (∼92 kcal mol^{-1}) and observing the fluorescence at 400 nm (∼71.5 kcal mol^{-1}), they have estimated the rate of energy transfer (k_{IEET}) from the observed differential circular anisotropy: $k_{IEET}(BOD) \geq 10^{10}$ s^{-1} and $k_{IEET}(TDD) \leq 10^{7}$ s^{-1}. These results clearly indicate that the energy transfer process is at least 1000 times more efficient in BOD.

The rate k_{IEET} in TDD is compatible with that predicted on the basis of dipole−dipole coupling (Förster model). On the other hand, if one compares transfer data in BOD with that obtained for flexible 1,4-aliphatic diketones ($k_{IEET} \geq 10^{8}$ s^{-1}),[17] the rate for BOD is much higher than for nonrigid diketones. While through-space Dexter-type interactions can be invoked to explain the rate of transfer in 1,4-diones, the rate in BOD could only be explained via a through-bond superexchange model. Because of this difference in behavior, these molecules constitute good prototype models for the experimental and theoretical study of intramolecular electronic energy transfer.

In this article, a static and dynamic theoretical study of BOD and TDD is presented. The structures and energetics of the first

† IRSAMC.
‡ King's College London.

10.1021/jp015570f CCC: $22.00
Published on Web 04/02/2002

SCHEME 1

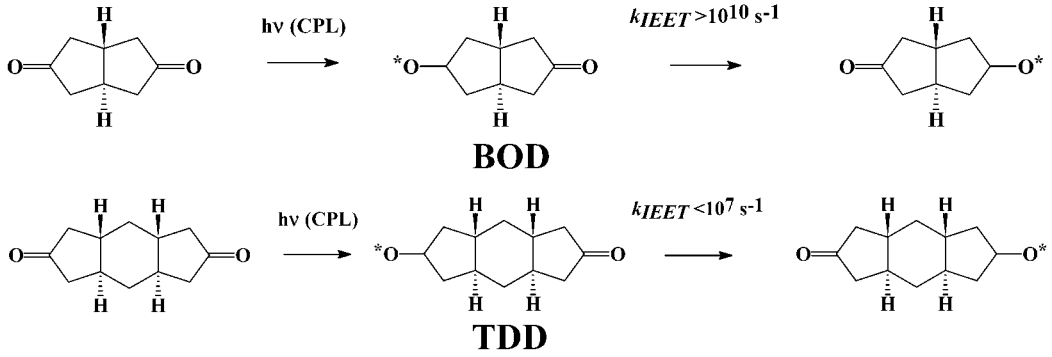

$n \rightarrow \pi^*$ excited states of both molecules are presented, to understand the nature of the potential energy surfaces. As will be discussed in detail, the first and second excited states are very close in energy in all regions of phase space that maintain C_{2h} molecular symmetry. The small difference from total degeneracy that emerges from these computations is explained in terms of weak interchromophoric electronic couplings. Since the energy splitting is very small, the nature of the IEET mechanism implies a nonadiabatic transition and involves a peculiar type of conical intersection. Thus, the conical intersections that are involved in radiationless decay processes for photochemical mechanisms[18−21] seem to be involved in IEET in rigidly linked bichromophoric molecules as well.

We find that the calculated potential energy surfaces of BOD and TDD are similar and do not reflect the difference in behavior experimentally observed. Classical trajectories have therefore been used to study the details of the first moments of the energy transfer mechanism that follow specific excitation of one chromophore. Since the IEET process occurs experimentally in the nanosecond or larger time scale domain in these two diketones,[16] the aim of these dynamics calculations is not to reproduce experiment but rather to give more insight into the very first steps of the IEET mechanism. Only one trajectory with no initial momenta in any of the normal modes and no symmetry restrictions has been computed for each molecule. This trajectory is the simplest possible generalization of a minimum energy path where the geometry relaxes under the force field of the excited state. Thus, the mechanism of IEET is presented as a traditional chemical *reaction path* followed by the nuclei as the reaction progresses on the potential energy surface. Consequently, the objective is to show how the electronic excitation is transferred from one part of the molecule to another by elucidating the details of nuclear motion. Excitation of the molecule places the system on an excited potential surface where the force field experienced by the nuclei is different from the ground state. Accordingly, the nuclei relax from the Franck−Condon region to trace out a reaction path to the products. The study of the relaxation process in this way gives mechanistic information but can never yield a rate. Since only a small region of the phase space is explored by this way, the information is qualitative but complementary to the usual models used to fit experimental IEET data.

The qualitative picture of IEET that emerges from our computations indicates that the transfer process occurs in a double-well like potential energy surface as shown in Scheme 2. Since a seam of intersections separates these potential wells, the mechanism must involve a nonadiabatic transition. However, while this "last" step is photochemical, the first stage of the process that follows excitation is adiabatic and corresponds mainly to an intramolecular vibrational redistribution (IVR) process.

SCHEME 2

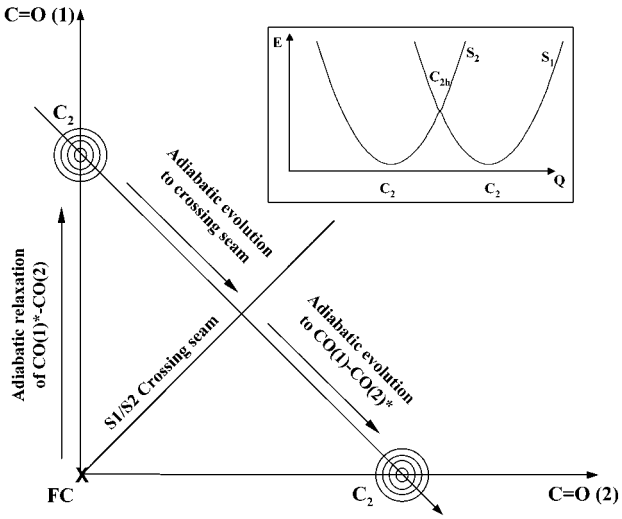

Computational Methods

All calculations for the ground and singlet excited states have been performed with the Gaussian 98 package[22] at the Complete Active Space Self-Consistent Field (CASSCF) level.[23]

To choose the correct minimal active space required to describe both diketones, a CASSCF study has been carried out on acetone, which represents the chromophore of the two molecular systems. Study of $n \rightarrow \pi^*$ excitation needs at least to take into account the π and π^* orbitals of the CO bond and the nonbonding n orbital associated with the oxygen lone pair. Then, one has to distribute 4 active electrons among these orbitals leading to a CAS(4,3) calculation. However, the equilibrium CO bond length of the $n \rightarrow \pi^*$ excited state is much longer (>0.1 Å) than in the ground state and this could affect the description of the CO σ bond. Consequently, one may want to allow for changes of the electronic structure in this bond explicitly in the CASSCF wave function[24] by adding one pair of σ and σ^* orbitals to the active space, leading to a CAS(6,5) calculation. The main goal of this preliminary study was to find the smallest active space necessary to reproduce the geometries and the excitation energies with sufficient accuracy, remembering that this active space will have to be doubled for the two diketones (giving either a CAS(8,6) or a CAS(12,10) calculation).

Full geometry optimizations of acetone have been performed for the ground state (S_0) and the first singlet $n \rightarrow \pi^*$ excited state (S_1). All results are given in Table 1 together with experimental[25−32] and additional theoretical data.[24,33−36] If one first considers calculations performed using the 6-31G(d) basis set,[37] both CASSCF ground-state geometries are in good

TABLE 1: Selected Experimental and Theoretical Bond Lengths (Å) for the Ground State (S_0) and the First Singlet $n \rightarrow \pi^*$ Excited State (S_1) of Acetone, Together with Vertical (ΔE_{vert}) and Adiabatic (ΔE_{adiab}) $S_0 \rightarrow S_1$ Excitation Energies (kcal mol^{-1}) (Experimental Bond Lengths and Excitation Energies from Refs 25−32)

	CO S_0	CC S_0	CO S_1	CC S_1	ΔE_{vert}	ΔE_{adiab}
Our Results						
CAS(4,3)/STO-3G	1.260	1.538	1.423	1.527	83.7	61.3
CAS(6,5)/STO-3G	1.282	1.536	1.464	1.524	84.3	62.9
CAS(4,3)/6-31G(d)	1.207	1.514	1.369	1.502	106.3	81.9
CAS(6,5)/6-31G(d)	1.227	1.511	1.401	1.506	114.4	89.6
Experimental Result[25−32]						
	1.215	1.515			100.9	86.5
	1.222	1.507			103.9	86.9
Other Theoretical Result						
CAS(4,3)/6-31G(d)[33]	1.207	1.514			106.3	
CAS(6,7)/ANO[24]	1.226	1.51			131.9	83.9
CAS(8,7)/D95[34]	1.228	1.520	1.399	1.507	118.9	95.2
DFT-LDA[35]	1.218	1.491	1.298	1.495	99.8	88.8
DFT-BLYP[35]	1.228	1.522	1.341	1.524	90.6	78.6
MNDC-CI[36]	1.220	1.530	1.310	1.500	75.4	62.5

agreement with experiment, with a CO bond length that is slightly too large (up to 0.012 Å for CAS(6,5)) or too small (up to 0.015 Å for CAS(4,3)). On the other hand, because no experimental data exist for the S_1 excited-state geometry of acetone yet, one can only compare the results to other theoretical data or to the experimental geometries obtained for formaldehyde[25,38] (CO bond length = 1.323 Å) or acetaldehyde[39] (CO bond length = 1.320 Å). The CAS(6,5) S_1 geometry is in good agreement with CAS(8,7)/D95 results but has a CO bond length larger than DFT, MNDO-CI and experimental data. On the other hand, the CO bond length obtained at the CAS(4,3) level is 0.03 Å shorter than previous CASSCF calculations but remains larger than the other theoretical and experimental geometries. While CO bond lengths are different when one uses various active spaces, the bond length difference between S_0 and S_1 geometries remains almost identical at both level of calculation ($CO(S_1)-CO(S_0)$ = 0.182 and 0.174 Å at the CAS(4,3) and CAS(6,5) levels of theory, respectively).

If one considers the $S_0 \rightarrow S_1$ vertical excitation, our calculated energies are too high compared to experimental results (max. error = 13.5 kcal mol^{-1}). This is partially due to the CASSCF method not including dynamic electron correlation. The inclusion of this effect will lower the energies of valence states toward better excitation energies.[40−42] On the other hand, adiabatic excitation energies are in better agreement with experimental results (max. error = 5 kcal mol^{-1}). According to these results, the CAS(4,3) active space can be considered sufficient to describe acetone, giving good geometries and excitation energies with a minimum computational effort.

One of the main goals of this work is to perform classical dynamical calculations on the S_1 potential energy surface (PES) at the CASSCF level for both diketone molecules. This implies a tremendous computational effort because a large number of points (energy, gradient and second derivatives) need to be calculated for each trajectory. Although a minimal active space was chosen, it proved impossible to compute trajectories for BOD and TDD using the 6-31G(d) basis set. Consequently, computations using the STO-3G basis set,[37] which is the smallest basis set available, have been performed and the results are given in Table 1. CO bond lengths for S_0 and S_1 states are ∼0.06 Å larger than the same bond lengths optimized using the 6-31G(d) basis set. One can observe the same tendency for CC bonds, the bond length increase being ∼0.02 Å. Furthermore, vertical and adiabatic excitation energies are ∼20 kcal mol^{-1} lower at the CAS(4,3) level compared to those obtained using the 6-31G(d) basis set. While the STO-3G results are not in agreement with experimental and other theoretical data, the general shape of the potential energy surfaces is qualitatively well described. The main differences are geometries shifted toward longer bond lengths, and the S_1 PES totally shifted toward lower energies. This last shift is not important in this study, because the analysis of $S_1 \rightarrow S_0$ decay is not the purpose of this work. The S_1 potential energy surface remains well above S_0 so no interaction with the ground state will appear. Thus the strategy has been to analyze the PES of both diketones at the CAS(8,6) level using 6-31G(d) and STO-3G basis sets, with only the CAS(8,6)/STO-3G method being used for trajectory calculations.

Finally, the S_1/S_2 energy difference for BOD has been calculated at the DDCI level,[43,44] which is implemented in the CASDI program.[45] This method performs a CASSCF calculation (CAS(8,6) in this case) in addition with all possible mono- and diexcitations except those involving two nonactive orbitals. The energy gap is almost identical to that found by previous CASSCF calculations, and no orbitals other than those directly involved in the CAS (π, n and π^* of both carbonyl groups) appear in the mono- and diexcitations manifold, thus confirming the validity of our choice of active space for CASSCF.

Studies of the short time scale excited-state relaxation following the specific vertical excitation of one chromophore were carried out for both diketones. Full quantum dynamics calculations using exact or fitted potential energy surfaces are not computationally feasible in our case, if one considers the number of degrees of freedom involved for each molecule. Consequently, classical trajectories were calculated "on the fly" on the S_1 potential energy surface directly from CAS(8,6)/STO-3G computations. Energy, gradient and second derivatives (Hessian) were calculated quantum mechanically along the trajectory, while nuclear propagation was performed by solving the classical Newton equations. The algorithm of Schlegel et al.,[46] currently available in the Gaussian 98 package, was used. The nuclear propagation was performed using a predictor-corrector method that needs a Hessian calculation at each step along the trajectory. While the Hessian computation can be very time-consuming, it allows the use of a larger time step than in standard predictor-corrector algorithms (1−2 fs in this work). A slightly modified Franck−Condon geometry was chosen as the starting point of the trajectories (see Results and Discussion section for more details) and no initial kinetic energy was added. Because the S_1/S_2 energy difference is very small for the starting geometries, state-averaged orbitals were used at the beginning of each trajectory. When this energy difference reached a value greater than 0.03 au during the trajectory, the state-averaging was progressively switched off, and the rest of the simulation performed only on the S_1 potential energy surface.

Results and Discussion

I. Ground-State Minima, Vertical Excitations, and Electronic Couplings. Ground-state geometry optimizations have been carried out with C_{2h} symmetry for BOD and TDD. The carbonyl group (CO) bond lengths of these minima (labeled S_0C_{2h}) are given in Table 2. At the same level of theory, the two molecules exhibit almost identical CO bond lengths. However, these are 0.006 Å shorter than those calculated for acetone (see Table 1).

Vertical excitation energies to the first two singlet $n \rightarrow \pi^*$ excited states S_1 and S_2 have been calculated and the results are given in Table 3. The correct excited electronic states of

TABLE 2: Bond Lengths (Å) and Pyramidalization Angles (α, Deg) of Carbonyl Groups Obtained by CASSCF Geometry Optimizations on the S_0 and S_1 Potential Energy Surfaces of the Two Bichromophoric Molecules BOD and TDD

	S_0 C_{2h}	S_1 C_{2h}	S_1 C_2	S_1 C_1
		BOD(STO-3G)		
C═O(1)	1.2541	1.3340	1.2540	1.2540
C═O(2)	1.2541	1.3340	1.4166	1.4171
α(1)	0.0	0.0	0.0	0.0
α(2)	0.0	0.0	0.0	35.1
		TDD(STO-3G)		
C═O(1)	1.2547	1.3343	1.2547	1.2547
C═O(2)	1.2547	1.3343	1.4165	1.4178
α(1)	0.0	0.0	0.0	0.0
α(2)	0.0	0.0	0.0	32.2
		BOD(6-31G(d))		
C═O(1)	1.2010	1.2718	1.2009	1.2009
C═O(2)	1.2010	1.2718	1.3578	1.3545
α(1)	0.0	0.0	0.0	0.0
α(2)	0.0	0.0	0.0	34.5
		TDD(6-31G(d))		
C═O(1)	1.2022	1.2723	1.2023	1.2023
C═O(1)	1.2022	1.2723	1.3521	1.3604
α(1)	0.0	0.0	0.0	0.0
α(2)	0.0	0.0	0.0	30.4

TABLE 3: S_1 and S_2 Excitation Energies (kcal mol^{-1}) Calculated for Various Local Minimum Geometries on the S_0 and S_1 Potential Energy Surfaces of BOD and TDD[a]

	S_0 C_{2h}	S_1 C_{2h}	S_1 C_2	S_1 C_1
		BOD(STO-3G)		
S_1	86.7130	76.4062	66.2263	61.8739
S_2	86.7794	76.4451		
		TDD(STO-3G)		
S_1	86.2214	76.0137	65.8811	61.4354
S_2	86.2236	76.0149		
		BOD(6-31G(d))		
S_1	113.4947	104.6844	87.2981	84.1572
S_2	113.8589	104.9126		
		TDD(6-31G(d))		
S_1	113.6023	104.8052	86.5814	83.7721
S_2	113.6059	104.8071		

[a] For each molecule and each basis set, the energetic reference (0.0 kcal mol^{-1}) is the S_0 energy calculated at the corresponding ground-state minimum geometry.

two identical coupled chromophores are the stationary-state wave functions $1/2^{1/2}(|A^*B\rangle \pm |AB^*\rangle)$, which represents a splitting of the single-molecule excited-state potential energy surface by twice the electronic coupling (also called the resonance term) $V = \langle A^*B|H|AB^*\rangle$.[47] Thus, molecular orbitals (MOs) are delocalized over the two carbonyl groups (see Figure 1 for the corresponding MOs in BOD) and calculation of the S_1/S_2 energy splitting is directly related to electronic coupling.

To investigate the influence of through-space and through-bond interactions, vertical excitation energies to S_1 and S_2 ($n \rightarrow \pi^*$ excitations) for formaldehyde dimers (denoted DIM(BOD) and DIM(TDD)) have been calculated. These dimers were obtained by removing the alkyl bridge from BOD and TDD but leaving the C═O groups in the same position. The S_1/S_2 energy splittings calculated at the STO-3G and 6-31G(d) level for BOD, TDD and the two resulting formaldehyde dimers are given in Table 4. All energy gaps are very small and must be treated with extreme care. Nevertheless, these very weak electronic couplings are consistent with experimental observations.[16] The values obtained for TDD and DIM(TDD) are in the domain of computational errors ($\sim 10^{-6}$ a.u.) and the comparison of these energy gaps is not meaningful. Through-space Dexter type and through-bond interactions are thus almost negligible and cannot be invoked to explain the rate of energy transfer experimentally observed for TDD as previously stated. On the other hand, S_1/S_2 energy differences obtained for BOD and DIM(BOD) are 10 to 100 times larger compared to TDD and DIM(TDD), depending on the basis set used. This observation is in agreement with the behavior of the electronic coupling as a function of the interchromophoric distance (C−C bond lengths ~7.1 and 4.5 Å for TDD and BOD, respectively).

In the case of BOD, the S_1/S_2 energy gap depends only on through-space and through-bond interactions and thus can be partitioned in two terms: $\Delta E\ (S_1/S_2) = \Delta E_{TS} + \Delta E_{TB}$, where ΔE_{TB} and ΔE_{TS} are the contributions to the total energy splitting of through-bond and through-space interactions respectively.[48] The value of ΔE_{TS} is directly obtained from the energy splitting of DIM(BOD). The use of the 6-31G(d) extended basis set increases the value of the energy gap by a factor 10 and by a factor 5 in the formaldehyde dimer and in BOD, respectively, compared to that obtained with the STO-3G basis set. While

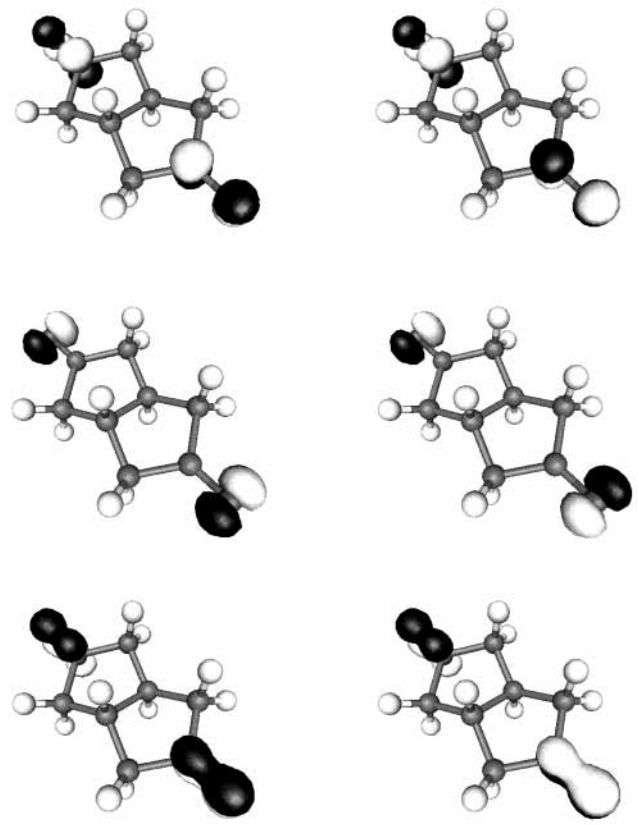

Figure 1. *n* (middle part), π (lower part), and π^* (upper part) molecular orbitals of BOD calculated at the CAS(8,6)/STO-3G level for the S_0C_{2h} geometry. The left and right side correspond to the $|A^*B\rangle + |AB^*\rangle$ and $|A^*B\rangle - |AB^*\rangle$ stationary states, respectively. Coefficients with absolute values larger than 0.05 have been used for the graphical representation.

TABLE 4: S_1/S_2 Energies Splitting $\Delta E = 2V$ (a.u.) Calculated at the Franck−Condon Geometries for Real Systems (BOD and TDD) and Formaldehyde Dimers Derived from the BOD and TDD Geometries (i.e., DIM(BOD) and DIM(TDD))

	BOD		TDD	
	STO-3G	6-31G(d)	STO-3G	6-31G(d)
real system	1.1×10^{-4}	5.8×10^{-4}	3.6×10^{-6}	5.7×10^{-6}
H_2CO dimer	1.1×10^{-5}	1.2×10^{-4}	7.6×10^{-7}	3.1×10^{-6}

STO-3G is suitable to describe short-range interactions, sizable errors on the energy gaps (and consequently on the electronic couplings) are found. These errors are corrected by the 6-31G(d) basis set that is suitable for long-range interactions occurring over distances greater than 3 Å.

To gain more insight into through-bond interactions, one needs to compare the energy gap calculated for BOD with the one found for DIM(BOD). Taking through-bond interactions into account gives much larger values than can be accounted for by direct through-space interactions between carbonyl groups (see Table 4). Using 6-31G(d), 80% of the total electronic coupling is provided by through-bond interactions. While the absolute values of electronic couplings are too small, this tendency is reproduced at the STO-3G level with a ratio $\Delta E_{TB}/\Delta E$ (S_1/S_2) equals to 90%. In fact, the through-space contribution to electronic coupling is negligible and the short-range Dexter model is not suitable to understand the rate of energy transfer observed for BOD.

Nevertheless, the small S_1/S_2 energy separation found for BOD and TDD (<0.4 kcal mol^{-1}) suggests that one part of the IEET process is nonadiabatic because these separations are smaller than the value of 0.6 kcal mol^{-1} given as a limit for the adiabatic regime.[49] If one considers the nonadiabatic weak coupling regime,[50] application of the Fermi Golden Rule leads to the following expression for the rate of energy transfer:[51]

$$k_{IEET} = 4\pi^2/h|V|^2\text{FCWD}$$

where V refers to the electronic coupling and FCWD to the Franck−Condon weighted density of states. Accordingly, if one wants to compare the k_{IEET} rates of two molecules, one needs to calculate the following ratio:

$$k_{IEET}(1)/k_{IEET}(2) = (|V_1|/|V_2|)^2(\text{FCWD}_1/\text{FCWD}_2)$$

In the first approximation, we have considered that $\text{FCWD}_{(BOD)} = \text{FCWD}_{(TDD)}$. This gives a k_{IEET}(BOD)/k_{IEET}(TDD) ratio approximately equal to 900 and 10000 using STO-3G and 6-31G(d) basis sets, respectively. This is in good and surprising agreement with experimental data (k_{IEET}(BOD)/k_{IEET}(TDD) ≥ 10^3)[16] considering that the FCWD factors have been neglected in the determination of the ratio and that the CASSCF calculations do not include dynamical correlation.

II. First Singlet Excited-State (S_1) Potential Energy Surface and Surface Crossings. Geometry optimizations on the S_1 potential energy surface have been carried out using STO-3G and 6-31G(d) basis sets with C_{2h}, C_2 or C_1 symmetry constraints. The corresponding BOD and TDD bond lengths and pyramidalization angles of the carbonyl groups are given in Table 2. The S_1 energies calculated for all corresponding minima are given in Table 3 and these values are relative to the S_0 energy determined for the corresponding S_0C_{2h} geometry.

For both molecules, a C_{2h} symmetry-constrained geometry optimization starting from the Franck−Condon (FC) structure leads to a local minimum (S_1C_{2h}) characterized by two identical CO bond lengths larger than those obtained for the S_0C_{2h} structure and molecular orbitals delocalized over the two chromophores. The increase of the CO bond lengths (0.07−0.08 Å) is almost identical for BOD and TDD with both STO-3G and 6-31G(d) basis sets (see Table 2). These "minima" lie 9−10 kcal mol^{-1} below the FC region of the S_1 PES for both molecules using the two chosen basis sets (see Table 3). Because the S_1 and S_2 surfaces are quasi-degenerate in the FC region, the energy of the second excited state (S_2) has been calculated for different structures chosen along the path followed by geometry optimizations (see Table 3 for S_1 and S_2 energies at S_0C_{2h} and S_1C_{2h} geometries).

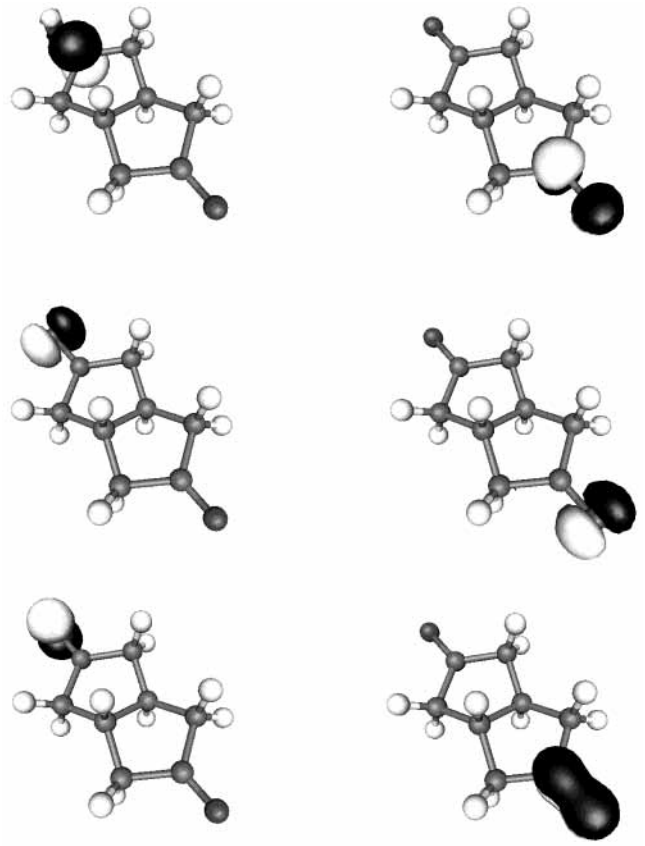

Figure 2. n (middle part), π (lower part), and π^* (upper part) molecular orbitals of BOD calculated at the CAS(8,6)/STO-3G level for the S_1C_2 geometry. Coefficients with absolute values larger than 0.05 have been used for the graphical representation.

The minimum point of degeneracy was optimized as a conical intersection (CI) between the S_1 and S_2 potential energy surfaces and corresponds exactly to the S_1C_{2h} structure found previously. From a general point of view, a conical intersection (where two potential energy surfaces cross) may appear as a sharp energy maximum on the lower potential energy surface when the energy is plotted along two particular coordinates: the gradient difference (GD) and the nonadiabatic derivative coupling (DC) vectors. These are the only two coordinates out of the $3N - 6$ geometric coordinates of the molecule that can split the energy degeneracy at the CI, thus leading to an $n - 2$-dimensional crossing where n is the total number degrees of freedom.[21] Unusually, the S_1C_{2h} structure located here is not a sharp energy maximum on the lower state: the gradients on both S_1 and S_2 are zero (Scheme 2), and hence the gradient difference is also zero.

At the S_1C_{2h} geometry, the derivative coupling coordinate is the antisymmetric stretching of the carbonyl groups that causes orbital localization (see Figure 2 for the corresponding MOs in BOD) and which, from a structural point of view, breaks the initial C_{2h} symmetry in C_2. Following the derivative coupling vector, two local minima (S_1C_2) have been optimized for each molecule, which lie ∼10 and ∼18 kcal mol^{-1} below the intersection when one uses STO-3G and 6-31G(d) basis sets, respectively. The S_1C_2 geometry is characterized by one excited carbonyl group with a longer CO bond length (Table 2) thus leading to a double-well like S_1 potential energy surface (Scheme 2). These structures have been characterized by frequency calculations and exhibit one low imaginary frequency

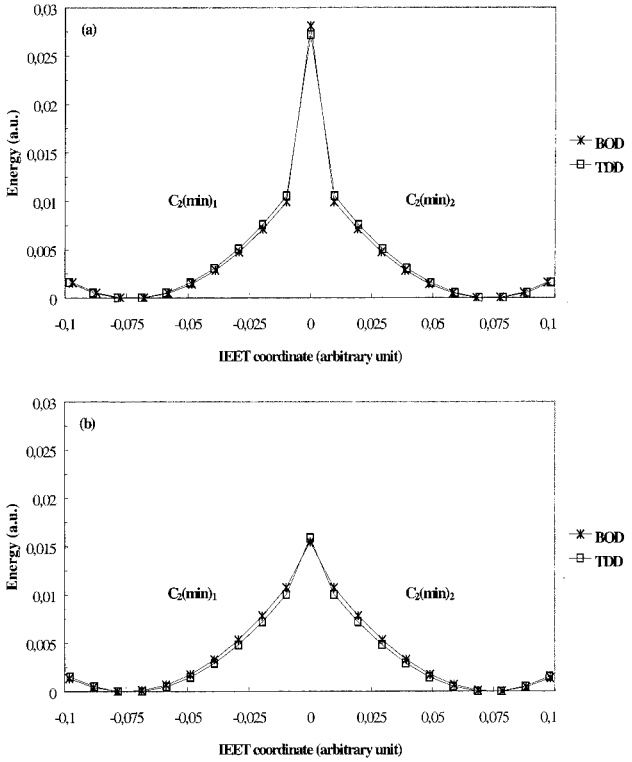

Figure 3. Energy profiles on S_1 determined by single point energy calculations at geometries obtained by following the derivative coupling vector that reflects the IEET reaction coordinate from the S_1C_{2h} geometry: (a) CAS(8,6)/6-31G(d) results; (b) CAS(8,6)/STO-3G results.

(330i−360i cm^{-1}), corresponding to pyramidalization of the excited carbonyl group. Following this vibrational normal mode, two minima of C_1 symmetry (S_1C_1) have been optimized for each molecule. These are characterized by one pyramidalized carbonyl group (above or below the mean plane of the molecule) and almost the same bond lengths as for S_1C_2 (See Table 2). From frequency calculations performed on these minima, one concludes that the S_1C_1 structures are real minima (no imaginary frequency). However, due to the low pyramidalization barrier (3−4 kcal mol^{-1}), the two S_1C_1 species may be in dynamic equilibrium, thus leading to a time-averaged S_1C_2 structure.

At S_1C_{2h}, the length of the gradient difference vector was found equal to zero for both molecules, indicating that the PES presents an $n-1$ dimensional "seam" of intersection (crossing) instead of an $n-2$ dimensional crossing.[52] This is in agreement with the conclusion about the nonadiabaticity of the IEET process suggested in the previous section. As a matter of fact, if one considers that the molecule travels from one well of the S_1 potential energy surface to the other one during the IEET process, then it must pass through the intersection seam, thus leading to a nonadiabatic transition. This nonadiabatic nature is reflected by the transfer coordinate Q given in Scheme 2. The reaction coordinate that localizes the molecular orbitals on each chromophore and thus reflects the energy transfer process is the derivative coupling vector. For either BOD or TDD, this reaction coordinate connects the two S_1C_2 potential wells via the S_1C_{2h} intersection and consequently implies the nonadiabaticity of the process. Determinations of the corresponding energy profiles have been performed by single-point calculations on geometries interpolated between the corresponding minima and the S_1C_{2h} structures. These energy profiles are given in Figure 3 for BOD and TDD. n and π^* orbital occupation numbers obtained directly from CASSCF calculations are plotted versus the transfer coordinate in Figure 4 (only STO-3G results for BOD are plotted, the 6-31G(d) calculations being identical). When the molecule is located in one S_1C_2 potential well (IEET coordinate between −0.1 and 0), $n(1)$ and $\pi^*(1)$ occupation numbers are equal to 1 ($n \rightarrow \pi^*$ excitation of chromophore (1)) while $n(2)$ and $\pi^*(2)$ occupation numbers are equal to 2.0 and 0.2, respectively (chromophore (2) in its ground-state configuration). On the other hand, the other S_1C_2 potential well (IEET coordinate between 0 and 0.1) is characterized by $n(2)$ and $\pi^*(2)$ occupation numbers equal to 1 ($n \rightarrow \pi^*$ excitation of chromophore (2)) and $n(1)$ and $\pi^*(1)$ occupation numbers are equal to 2.0 and 0.2, respectively (chromophore (1) in its ground-state configuration). According to Figure 4, when one travels from one potential well to the other, no transfer is detected along the IEET coordinate until the molecule reaches the S_1C_{2h} structure where the excitation is transferred "instantaneously" which is in agreement with the nonadiabatic character of the process.

The transfer process and the description of the potential energy surfaces where the transfer occurs are similar to those found in the bismethyleneadamantane radical cation (BMA) which exhibits intramolecular electron transfer.[52] Like BOD or TDD, BMA is a symmetrical rigidly linked bichromophoric molecule showing a collinear orientation of chromophores identical to that found in BOD and TDD. The same conclusions have been reached for the BMA radical cation and for the two bichromophoric model compounds BOD and TDD: the double-well like potential energy surfaces exhibit a seam of intersections and, consequently, the transfer processes are nonadiabatic.

III. Dynamics Calculations. From the analysis of the S_1 potential energy surfaces, the differences between BOD and TDD do not appear to be significant. The only feature that differentiates these two molecules is the existence of very weak interchromophoric electronic couplings in BOD, which slightly splits the S_1 and S_2 potential energy surfaces for C_{2h} geometries. However, these couplings are not large enough to allow a significant modification of the BOD S_1 potential energy surface compared to TDD. Static information, i.e., the shape of the potential energy surface is not adequate to explain the difference in the experimental energy transfer rate constants between BOD and TDD. Consequently, an exploration of the dynamical aspects of intramolecular energy transfer in these two molecular systems is necessary.

The purpose of these calculations is not to reproduce the energy transfer process but rather to show how the existence of through-bond interactions modifies the dynamic behavior of each molecule. As stated in the previous sections, excitation to S_1 at the Franck−Condon geometry leads to the excitation of both chromophores because of the C_{2h} symmetry and the corresponding MO delocalization. Consequently, trajectory calculations have been started from modified Franck−Condon geometries on the S_1 potential energy surface in order to reproduce specific excitation of one chromophore. The CO bond length and pyramidalization angle of only one chromophore (noted CO(1)) have been slightly enlarged while the other carbonyl group (noted CO(2)) was kept in its ground-state geometry. Thus, this starting geometry maintains the molecule close to the Franck−Condon region while ensuring the specific excitation of only one chromophore. Trajectory calculations have been performed using a time step lower than 2 fs and reproduce a 1.3 ps time evolution for both molecules.

The behavior of CO(1) and CO(2) bonds in BOD and TDD is shown in Figure 5 for a time evolution of 200 fs. For both molecules, one sees (x-axis) a complete relaxation of the initially excited chromophore through the corresponding S_1 minimum,

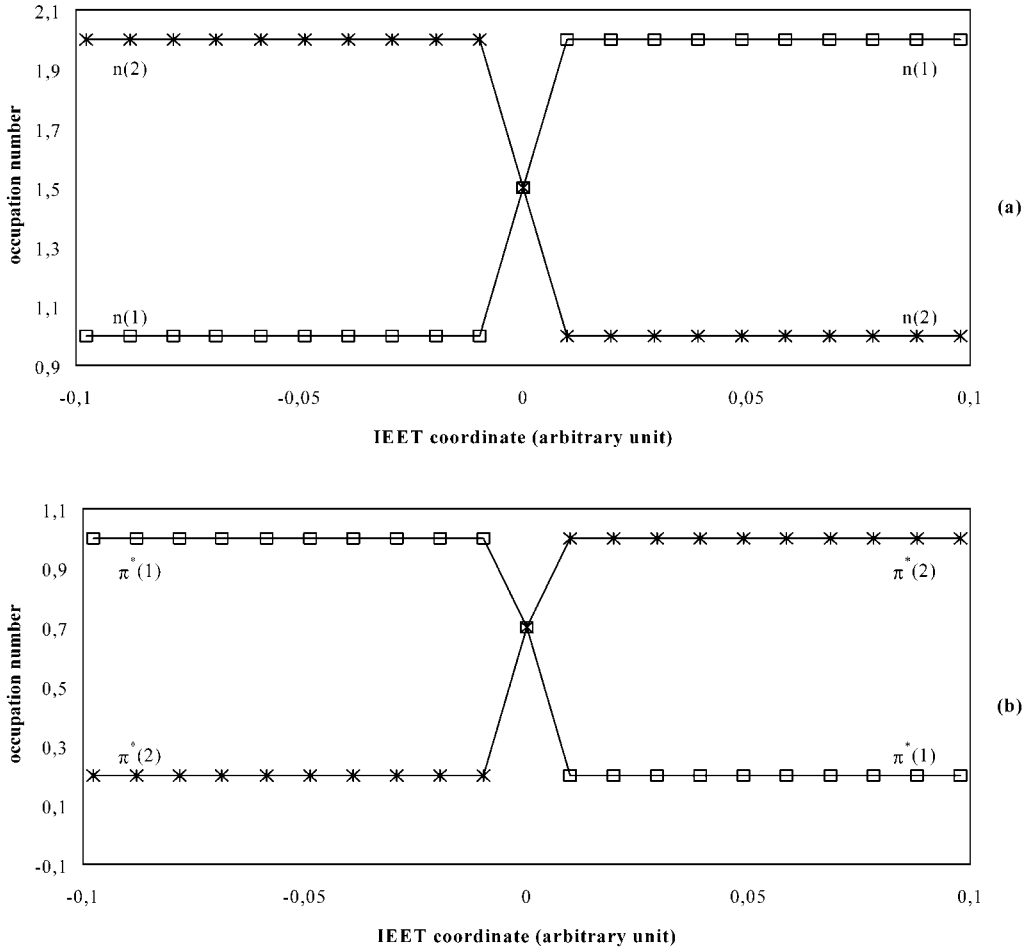

Figure 4. Occupation numbers of n (a) and π^* (b) orbitals as a function of the IEET reaction coordinate calculated for BOD at the CAS(8,6)/STO-3G level. The number in parentheses is used to discriminate between both chromophores.

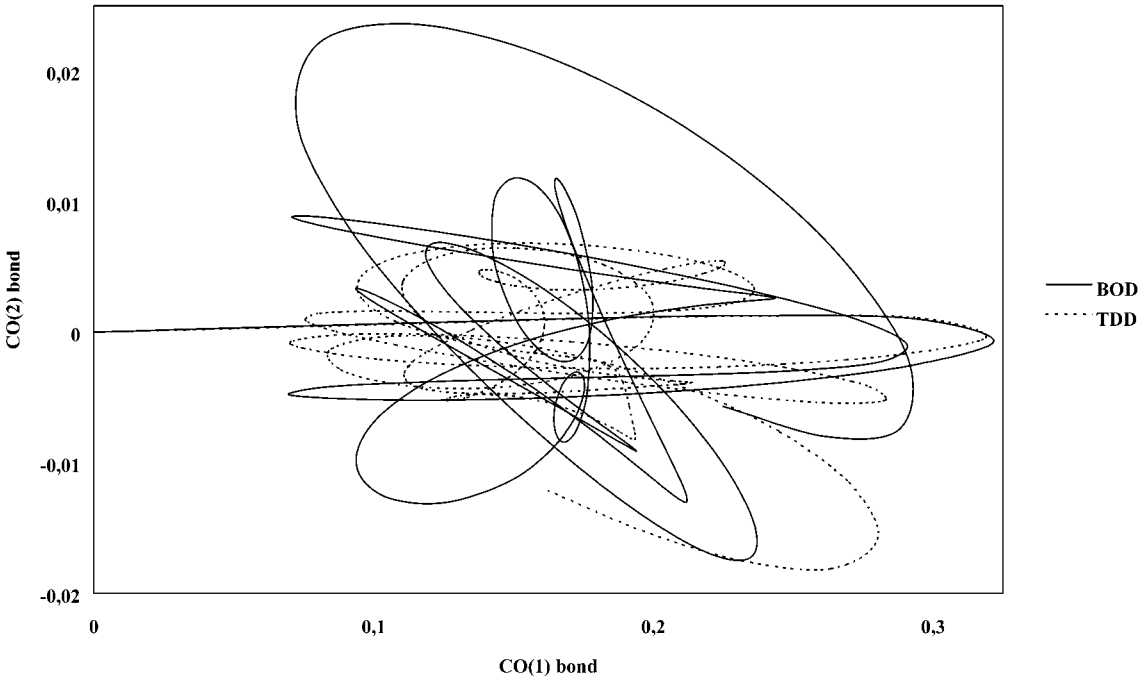

Figure 5. Initially excited chromophore (x-axis) vs initially nonexcited chromophore (y-axis) bond length difference (Å) relative to the starting point of the trajectory (0, 0). Trajectory for BOD is represented with a solid line while the TDD simulation is shown with a dashed line.

coupled with much smaller modifications of the other (non-excited) chromophore geometry (y-axis). The small modification of the CO(2) bond length is 2 times larger in BOD than in TDD. Thus, even for this short time scale, one observes the flow of energy into the CO(2) coordinate at a faster rate for BOD compared to TDD. As has been previously discussed, the

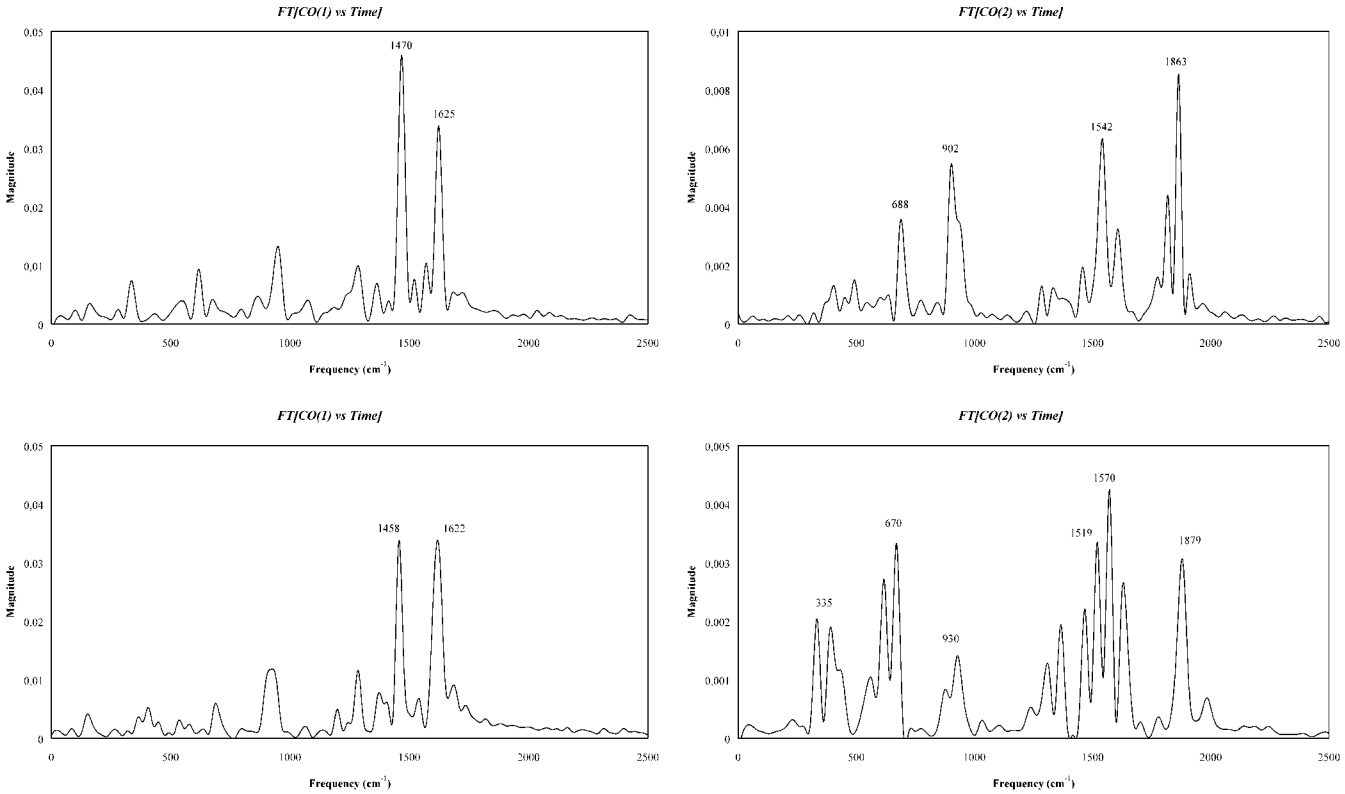

Figure 6. BOD (upper part) and TDD (lower part) frequency spectra obtained by Fourier transform of CO bond length time evolution. The left side corresponds to spectra obtained for initially excited CO(1) chromophore and the right side to initially nonexcited CO(2) moiety.

interchromophoric coupling is larger for BOD due to more efficient interactions. Thus, the origin of the dynamical behavior can be related to the existence of weak interchromophoric couplings.

To obtain more insight into dynamical aspects of the IEET transfer process, frequency spectra have been calculated by performing a Fourier transform of the evolution of the bond lengths of both carbonyl groups as a function of time (Figure 6). For this purpose the whole trajectory has been used, corresponding to a 1.3 ps time evolution.

For the initially excited chromophore (CO(1)), the bond length oscillations are characterized by two specific eigenfrequencies, which are almost identical for BOD and TDD. These frequencies (1468 and 1625 cm^{-1} for BOD; 1457 and 1619 cm^{-1} for TDD) can be associated to vibrational normal modes that have been calculated at the global minimum geometry (S_1C_1) on the S_1 potential energy surface of both molecules. The 1468 and 1625 cm^{-1} normal modes determined by frequency calculation for BOD at the STO-3G level (which are equal to those obtained by a Fourier analysis) correspond to the stretching of the CO(1) bond together with the motion of various atoms of the bridge (Figure 7). The atoms involved in these vibrational modes are mainly localized in a region of the molecule that is close to the excited carbonyl group and the associated nuclear motions involve only this half of the molecule. The same observations arise when one considers the 1472 and 1634 cm^{-1} normal modes obtained by frequency calculation on the S_1 minimum S_1C_1 of TDD (Figure 8). Thus, the vibrational regime of the alkyl bridge is intimately linked to that of CO(1). Indeed, when the CO(1) bond relaxes, vibrational energy is partly transferred to one side of the bridge that is directly linked to this chromophore. If one uses the classical mechanical analogy of a vibrating spring, this oscillatory motion must propagate itself from one side of the molecule (the excited CO(1) chromophore) through the σ-bond framework and must finally reach the other side of the molecule (the nonexcited CO(2) chromophore). In the end, these phenomena will induce vibrational excitation of CO(2) bond.

The bond length evolution of the initially nonexcited chromophore CO(2) is characterized by different eigenfrequencies from those obtained for CO(1). The spectrum obtained by Fourier analysis for BOD mainly involves four different frequencies (Figure 6). The one that has the largest magnitude is located at 1863 cm^{-1} and must correspond exactly to the 1863 cm^{-1} frequency calculated at the S_1C_1 geometry. The associated vibrational normal mode corresponds to the CO(2) stretch (Figure 7). On the other hand, the three other frequencies (688, 902, 1542 cm^{-1}) are only characterized by vibrational motions of bridge atoms. These atoms are essentially located on the bridge that is closest to the CO(2) carbonyl group. In the TDD case, a more complex frequency spectrum arises from Fourier transform. The 1879 cm^{-1} frequency that corresponds to the CO(2) stretching mode calculated at 1868 cm^{-1} at the S_1C_1 geometry is not the most intense in the frequency spectrum (Figure 6). On the other hand, the frequencies that characterize the TDD spectrum involve alkyl atom motions. One may conclude that the oscillatory behavior of the initially nonexcited chromophore of BOD is mainly characterized by CO(2) bond stretching after 1.3 ps, while for TDD the vibrational excitation of this normal mode is less important.

Using these results, a schematic explanation of the intramolecular process can be developed in order to understand how electronic excitation energy is transferred in these bichromophoric molecules. After excitation of one carbonyl group (CO(1)), the first step of the process is an adiabatic vibrational relaxation of CO(1) along the corresponding potential well in the S_1 potential energy surface (Scheme 2). Then, there is a progressive propagation of vibrations from one side of the molecule to the other one through the σ-bonded framework. During the dynamical process, the amplitude of the CO(1) oscillations progressively decreases while those of CO(2)

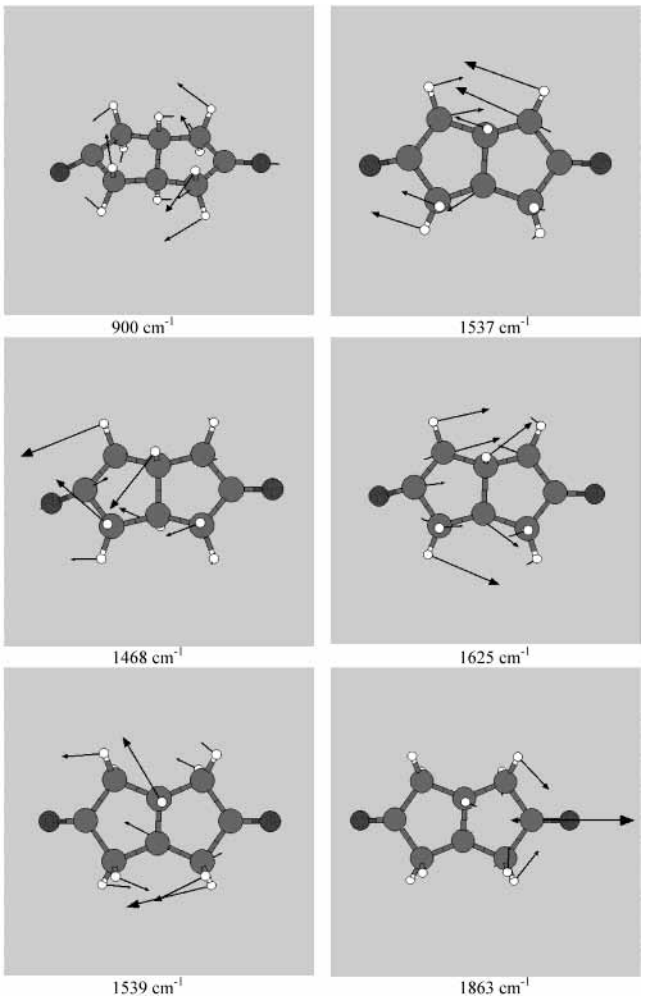

Figure 7. Selected vibrational normal modes of BOD calculated at the CAS(8,6)/STO-3G level for S_1C_1 geometry. The threshold used for the vector representation of nuclear motion is the same for all normal modes.

increases at the same time. Thus, the molecule "travels" from one potential well of the S_1 PES toward the other one and passes through the crossing seam where nonadiabatic energy transfer can take place (Scheme 2). One can then consider the IEET process as an intramolecular vibrational redistribution (IVR) that propagates the vibrations from the excited chromophore to the other one, the bridge acting as a medium on which the vibration travels. It is clear that, with more σ-bonds, the transfer process will be slower. The σ-bond bridge not only enhances interchromophoric electronic coupling via through-bond interactions compared to through-space interactions, it also controls the IEET process by promoting IVR from one side of the molecule into the other.

Conclusions

Intramolecular electronic energy transfer (IEET) in aliphatic diketones that contain rigidly linked carbonyl group chromophores has been studied by means of potential energy surface analysis and classical trajectory simulations. We have shown that two geometric coordinates (the carbonyl bond lengths) and two singlet diabatic states (characterized by the specific excitation of either one chromophore or the other) are needed to understand the mechanism of IEET in these systems.

While interchromophoric exchange and through-bond interactions are larger in BOD than in TDD, static calculations at the

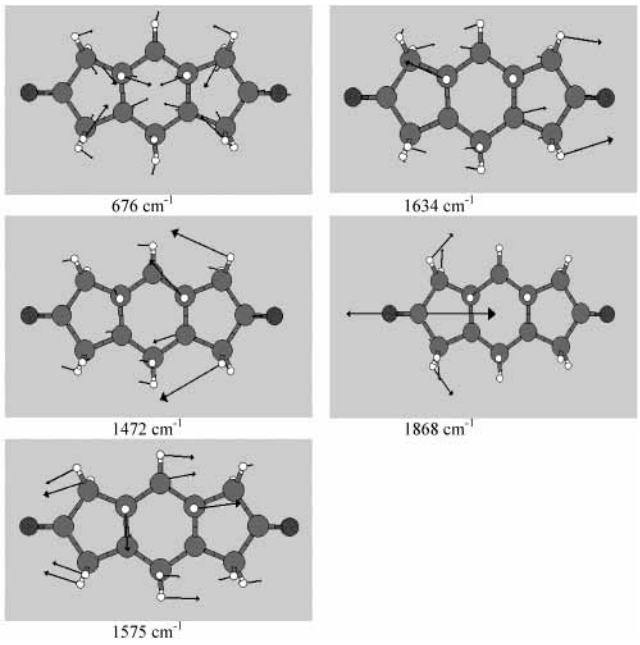

Figure 8. Selected vibrational normal modes of TDD calculated at the CAS(8,6)/STO-3G level for the S_1C_1 geometry. The threshold used for the vector representation of nuclear motion is the same for all normal modes.

CASSCF level have not shown significant differences between the double-well type S_1 potential energy surfaces of both molecules. Moreover, these interactions are not large enough to allow a significant splitting of the two first adiabatic excited states in the configuration space of C_{2h} symmetry. Thus, the main characteristic of these surfaces is an S_1/S_2 seam of intersection that appears for all C_{2h} symmetry geometries. Consequently, the molecules must travel through a region of surface crossing during the IEET process, which thus involves a nonadiabatic transition. However, dynamics calculations have shown that the first step of IEET is mainly an adiabatic mechanism of intramolecular vibrational redistribution (IVR) into the initially nonexcited chromophore vibrations. It is worth noting that this conclusion has also been reached in a recent theoretical work on IEET in 9-anthryl-1′-naphthylalkanes.[53]

The whole picture that emerges from these results is that this IEET process can be divided into two principal parts. The first step corresponds to an adiabatic complete relaxation of the initially excited chromophore. During this relaxation process, the associated vibrational motion, initially located on the excited carbonyl group, propagates itself progressively through the alkyl bridge and reaches the initially nonexcited chromophore (IVR mechanism). Thus, one sees that the σ-bond bridge not only enhances interchromophoric electronic coupling via through-bond interactions compared to through-space interactions, it also controls the IEET process by promoting IVR from one side of the molecule into the other. In the present case, one clearly observes that IVR is slower in the molecule characterized by the more extended σ-bonds bridge (TDD). To explain the IEET process in both molecules, one can use a vibrating spring analogy. The longer the spring (analogy to bridge size), the more time it takes for a vibration to travel from one side (chromophore) to the other one. The larger the spring force constant (analogy to electronic coupling), the higher the characteristic frequency of the spring and the faster the vibration travels. During the evolution of the molecule on the potential energy surface, the amplitude of the initially nonexcited chromophore vibrational motion will increase. According to this evolution

process and knowing that the molecule has enough energy to reach the minimum point of the S_1/S_2 intersection seam, one may consider that the second part of the whole IEET mechanism corresponds to the passage of the molecule through the region of surface crossing. Thus, the final step corresponds to a nonadiabatic transition from one potential well (excitation located on one chromophore) to the other (excitation located on the other chromophore).

Supporting Information Available: Cartesian coordinates of all BOD and TDD structures (S_0C_{2h}, S_1C_{2h}, S_1C_2, S_1C_1) optimized at the STO-3G and 6-31G(d) level. This material is available free of charge via the Internet at http://pubs.acs.org.

References and Notes

(1) Speiser, S. *Chem. Rev.* **1996**, *96*, 1953−1976.
(2) Förster, Th. *Ann. Phys. (Leipzig)* **1948**, *2*, 5.
(3) Förster, Th. *Discuss. Faraday Soc.* **1959**, *27*, 7.
(4) Förster, Th. In *Modern quantum chemistry*; Sinanoglu, O., Ed.; Academic Press: New York, 1968; Vol. 3, p 93.
(5) Dexter, D. L. *J. Chem. Phys.* **1953**, *5*, 836−850
(6) McConnell, H. M. *J. Chem. Phys.* **1961**, *35*, 508.
(7) Hoffmann, R.; Imamura, A.; Hehre, W. J. *J. Am. Chem. Soc.* **1967**, *90*, 1499.
(8) Hoffmann, R. *Acc. Chem. Res.* **1971**, *4*, 19.
(9) Jordan, K. D.; Paddon-Row, M. N. *Chem. Rev.* **1992**, *92*, 395.
(10) Paddon-Row, M. N. *Acc. Chem. Res.* **1982**, *15*, 245.
(11) Paddon-Row, M. N.; Jordan, K. D. In *Modern models of bonding and delocalization*; Liebman, J. F., Ed.; VCH: New York, 1988.
(12) Paddon-Row, M. N.; Wong, S. S.; Jordan, K. D. *J. Am. Chem. Soc.* **1990**, *112*, 1710.
(13) Shephard, M. J.; Paddon-Row, M. N.; Jordan, K. D. *J. Am. Chem. Soc.* **1994**, *116*, 5328.
(14) Monberg, E. M.; Kopelman, R. *Chem. Phys. Lett.* **1978**, *58*, 492.
(15) Klafter, J.; Jortner, J. *Chem. Phys. Lett.* **1978**, *60*, 5.
(16) Schippers, P. H.; Dekkers, H. P. J. M. *J. Am. Chem. Soc.* **1983**, *105*, 145−146.
(17) Lissi, E. A.; Encinas, M. V.; Castañeda, F.; Olea, F. A. *J. Phys. Chem.* **1980**, *84*, 251−255.
(18) Teller, E. *Isr. J. Chem.* **1969**, *7*, 227−235.
(19) Zimmerman, H. E. *J. Am. Chem. Soc.* **1966**, *88*, 1566−1567.
(20) Michl, J. *J. Mol. Photochem.* **1972**, 243−255.
(21) Bernardi, F.; Olivucci, M.; Robb, M. A. *Chem. Soc. Rev.* **1996**, *25*, 321−328.
(22) Frisch, M. J.; Trucks, G. W.; Schlegel, H. B.; Scuseria, G. E.; Robb, M. A.; Cheeseman, J. R.; Zakrzewski, V. G.; Montgomery, J. A.; Stratmann, R. E., Jr.; Burant, J. C.; Dapprich, S.; Millam, J. M.; Daniels, A. D.; Kudin, K. N.; Strain, M. C.; Farkas, O.; Tomasi, J.; Barone, V.; Cossi, M.; Cammi, R.; Mennucci, B.; Pomelli, C.; Adamo, C.; Clifford, S.; Ochterski, J.; Petersson, G. A.; Ayala, P. Y.; Cui, Q.; Morokuma, K.; Malick, D. K.; Rabuck, A. D.; Raghavachari, K.; Foresman, J. B.; Ortiz, J. V.; Cioslowski, J.; Stefanov, B. B.; Liu, G.; Liashenko, A.; Piskorz, P.; Komaromi, I.; Gomperts, R.; Martin, R. L.; Fox, D. J.; Keith, T.; Al-Laham, M. A.; Peng, C. Y.; Nanayakkara, A.; Gonzalez, C.; Challacombe, M.; Gill, P. M. W.; Johnson, B.; Chen, W.; Wong, M. W.; Andres, J. L.; Gonzalez, C.; Head-Gordon, M.; Replogle, E. S.; Pople, J. A. *Gaussian 98*, revision A.6; Gaussian, Inc.: Pittsburgh, PA, 1998.
(23) Roos, B. O. In *Adv. Chem. Phys. (Ab initio methods in quantum chemistry, vol. II)*; Lawley, K. P., Ed.; Wiley: New York, 1987; Vol. 69, p 399−446.
(24) Merchan, M.; Roos, B. O.; McDiarmid, R.; Xing, X. *J. Chem. Phys.* **1996**, *104*, 1791−1804.
(25) Harmony, M. D.; Laurie, V. W.; Kuczkowski, R. L.; Schwendeman, R. H.; Ramsay, D. A.; Lovas, F. J.; Lafferty, W. J.; Maki, A. G. *J. Phys. Chem. Ref. Data* **1979**, *8*, 619.
(26) Nelson, R.; Pierce, L. *J. Mol. Spectrosc.* **1965**, *18*, 344.
(27) Huebner, R. H.; Celotta, R. J.; Mielczarek, S. R.; Kuyatt, C. E. *J. Chem. Phys.* **1973**, *59*, 5434.
(28) Walzl, K. N.; Koerting, C. F.; Kuppermann, A. *J. Chem. Phys.* **1987**, *87*, 3796.
(29) Allinger, N. L.; Stuart, T. W.; Tai, J. C. *J. Am. Chem. Soc.* **1968**, *90*, 2809.
(30) Baba, M.; Hanazaki, I.; Nagashima, U. *J. Chem. Phys.* **1985**, *82*, 3938.
(31) Xing, X.; McDiarmid, R.; Philis, J. G.; Goodman, L. *J. Chem. Phys.* **1993**, *99*, 7565.
(32) Basch, H.; Robin, M. B.; Kuebler, N. A. *J. Chem. Phys.* **1967**, *47*, 1201.
(33) Cossi, M.; Barone, V. *J. Chem. Phys.* **2000**, *112*, 2427−2435.
(34) Sakurai, H.; Kato, S. *J. Mol. Struct. (THEOCHEM)* **1999**, *461*−*462*, 145−152.
(35) Frank, I.; Hutter, J.; Marx, D.; Parrinello, M. *J. Chem. Phys.* **1998**, *108*, 4060−4069.
(36) Klessinger, M.; Pötter, T.; Wüllen, C. V. *Theor. Chim. Acta* **1991**, *80*, 1.
(37) Description of basis sets can be found in the following: Foresman, J. B.; Frisch, A. E. In *Exploring chemistry with electronic structure methods*, 2nd Ed.; Gaussian Inc: Pittsburgh, 1998.
(38) Takagi, K.; Oka, T. *J. Phys. Soc. Jpn.* **1963**, *18*, 1174.
(39) Hubbard, L. M.; Bocian, D. F.; Birge, R. R. *J. Am. Chem. Soc.* **1981**, *103*, 3313.
(40) Andersson, K.; Malmqvist, P.-Å; Roos, B. O.; Salej, A. J.; Wolinski K. *J. Phys. Chem.* **1990**, *94*, 5483.
(41) Andersson, K.; Malmqvist, P.-Å; Roos, B. O. *J. Chem. Phys.* **1992**, *96*, 1218.
(42) McDouall, J. J.; Peasley, K.; Robb, M. A. *Chem. Phys. Lett.* **1988**, *148*, 183.
(43) Miralles, J.; Castel, O.; Cabayol, R.; Malrieu, J. P. *Chem. Phys.* **1993**, *172*, 39.
(44) Sanz, J. F.; Malrieu, J. P. *J. Phys. Chem.* **1993**, *97*, 99.
(45) Ben Amor, N.; Maynau, D. *Chem. Phys. Lett.* **1998**, *286*, 211−220.
(46) Chen, W.; Hase, W. L.; Schlegel, H. B. *Chem. Phys, Lett.* **1994**, *228*, 436−442.
(47) McWeeny, R. In *Methods of molecular quantum mechanics*, 2nd ed.; Academic Press: New York, 1992; p 514−516.
(48) Scholes, G. D.; Ghiggino, K. P.; Oliver, A. M.; Paddon-Row, M. N. *J. Am. Chem. Soc.* **1993**, *115*, 4345−4349.
(49) Farazdel, A.; Dupuis, M.; Clementi, E.; Aviram, A. *J. Am. Chem. Soc.* **1990**, *112*, 4206.
(50) Fulton, R. L.; Gouterman, M. *J. Chem. Phys.* **1961**, *35*, 1059.
(51) Scholes, G. D.; Ghiggino, K. P. *J. Chem. Phys.* **1994**, *101*, 1251−1261.
(52) Blancafort, L.; Jolibois, F.; Olivucci, M.; Robb, M. A. *J. Am. Chem. Soc.* **2001**, *123*, 722−732.
(53) Jolibois, F.; Bearpark, M. J.; Klein, S.; Olivucci, M.; Robb, M. A. *J. Am. Chem. Soc.* **2000**, *122*, 5801−5810.